J. Fluid Mech. (2022), *vol*. 940, A32, doi:10.1017/jfm.2022.257

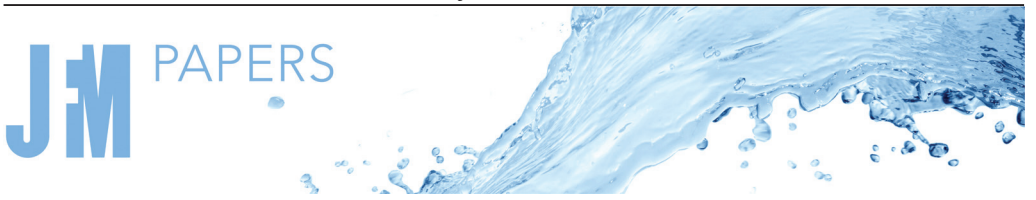

Theory of nonlinear acoustic forces acting on inhomogeneous fluids

Varun Kumar Rajendran[1], **Sujith Jayakumar**[1], **Mohammed Azharudeen**[1] and **Karthick Subramani**[1],†

[1]Department of Mechanical Engineering, Indian Institute of Information Technology, Design and Manufacturing, Kancheepuram, Chennai 600127, India

(Received 9 October 2021; revised 21 January 2022; accepted 12 March 2022)

Recently, the phenomena of streaming suppression and relocation of inhomogeneous miscible fluids under acoustic fields were explained using the hypothesis on mean Eulerian pressure. In this work, we derive the expression for the acoustic body force without relying on any prior assumptions regarding the second-order Eulerian pressure. We present a theory of nonlinear acoustics for inhomogeneous fluids from first principles, which explains streaming suppression and acoustic relocation in both miscible and immiscible inhomogeneous fluids inside a microchannel. This theory predicts the relocation of higher impedance fluids to pressure nodes of the standing wave, which agrees with recent experiments.

Key words: acoustics, micro-/nano-fluid dynamics, low-Reynolds-number flows

1. Introduction

The acoustic fields imposed on fluids exhibit several interesting nonlinear acoustic phenomena including an acoustic radiation force acting on particles or interfaces, and acoustic streaming (Friend & Yeo 2011). This subject has a long history, beginning with early investigations by Faraday (1831), Rayleigh (1884), King (1934) and Lighthill (1978). Over the last two decades, employing these acoustic forces in microscale flows has become a rapidly growing research field known as 'acoustofluidics'. It has far-ranging applications in biological (Petersson *et al.* 2007; Wiklund 2012; Collins *et al.* 2015; Lee *et al.* 2015; Ahmed *et al.* 2016), medical (Augustsson *et al.* 2012; Li *et al.* 2015) and chemical sciences (Suslick *et al.* 1999; Li & Huang 2019; Chen *et al.* 2021). Recently, two interesting phenomena were observed in microchannel experiments: (i) inhibition of Rayleigh streaming vortices (bulk flow rolls outside the boundary layer due to interaction of the acoustic wave with a solid boundary) called acoustic streaming suppression and

† Email address for correspondence: karthick@iiitdm.ac.in

(ii) relocation or stabilization of inhomogeneous fluids to a stable configuration called acoustic relocation (Deshmukh *et al.* 2014; Augustsson *et al.* 2016). This phenomenon opens the door to several applications including sorting of submicron particles such as bacteria and nanoparticles using acoustofluidic systems (Gautam *et al.* 2018; Van Assche *et al.* 2020), tweezing and patterning of fluids (Karlsen & Bruus 2017; Baudoin & Thomas 2020) and on-demand stream to stream or stream to drop relocation of immiscible fluids (Hemachandran *et al.* 2019, 2021).

The main goal of this work is to develop a theory of nonlinear acoustics for inhomogeneous fluids that explains the phenomena of acoustic relocation and streaming suppression. Remarkably, our theory predicts that the acoustic relocation/stabilization of inhomogeneous fluids in a microchannel subjected to standing acoustic waves is possible only if there exists an impedance ($Z = \rho c$) gradient, which agrees well with recent experiments. We demonstrate that the amplitude of the first-order fields is highly dependent on fluid configuration, thus acoustic energy density (E_{ac}) varies significantly during the process of relocation and diffusion, whereas E_{ac} is assumed to be constant in previous works (Karlsen, Augustsson & Bruus 2016; Karlsen 2018). Also, we successfully separate the streaming term and acoustic relocation term from the generalized acoustic body force, which was previously claimed not to be possible by Karlsen *et al.* (2018). Furthermore, this theory also explains the recently observed relocation of immiscible fluids under acoustic fields (Hemachandran *et al.* 2019).

Although Karlsen *et al.* (2016) explained these phenomena using the acoustic force density, $f_{ac} = -\boldsymbol{\nabla}\cdot\langle p_2 I + \rho_0 \boldsymbol{v}_1\boldsymbol{v}_1\rangle$, it is not derived from first principles and involves the assumption on the time-averaged second-order mean Eulerian pressure as $\langle p_2\rangle = (1/2)[\kappa_0\langle|p_1|^2\rangle - \rho_0\langle|\boldsymbol{v}_1|^2\rangle]$, which is claimed as the central hypothesis of their theory (Karlsen 2018). Here, ρ_0 is the zeroth-order density, κ_0 is the zeroth-order compressibility, p_1 is the first-order pressure and $\boldsymbol{v}_1$ is the first-order velocity. The following are our objections to this assumption: first, like any other pressure field, the mean Eulerian pressure has to be derived from the Navier–Stokes (N-S) equations. Second, if the assumed p_2 is the second-order Eulerian pressure then the pressure that results from the N-S equations after the substitution of f_{ac} lacks clarity. In this work, we improve the clarity of the acoustic force density by deriving it from first principles without invoking any assumption on the time-averaged second-order mean Eulerian pressure $\langle p_2\rangle$.

2. Physics of the problem

The hydrodynamics of inhomogeneous fluids considered in this study is governed by the mass continuity, momentum and advection–diffusion equations (Landau & Lifshitz 1987)

$$\partial_t\rho + \boldsymbol{\nabla}\cdot(\rho\boldsymbol{v}) = 0, \tag{2.1a}$$

$$\rho[\partial_t\boldsymbol{v} + (\boldsymbol{v}\cdot\boldsymbol{\nabla})\boldsymbol{v}] = -\boldsymbol{\nabla}p + \eta\nabla^2\boldsymbol{v} + \beta\eta\boldsymbol{\nabla}(\boldsymbol{\nabla}\cdot\boldsymbol{v}) + \rho\boldsymbol{g}, \tag{2.1b}$$

$$\partial_t s + \boldsymbol{v}\cdot\boldsymbol{\nabla}s = D\nabla^2 s, \tag{2.1c}$$

where ρ is the density, $\boldsymbol{v}$ is the velocity, p is the pressure, η is the dynamic viscosity of the fluid, ξ is the bulk viscosity, $\beta = (\xi/\eta) + (1/3)$, g is acceleration due to gravity in negative y-direction ($\boldsymbol{g} = -g\boldsymbol{j}$), s is the solute concentration and D is the diffusivity. When the fluid is subjected to acoustic waves, the following thermodynamic pressure–density relation in terms of material derivative $(\mathrm{d}/\mathrm{d}t) = \partial_t + (\boldsymbol{v}\cdot\boldsymbol{\nabla})$ is also required

(Bergmann 2005):

$$\frac{\mathrm{d}\rho}{\mathrm{d}t} = \frac{1}{c^2}\frac{\mathrm{d}p}{\mathrm{d}t}, \tag{2.1d}$$

where $c^2 = (\partial p/\partial\rho)|_S$ and c is the adiabatic local speed of sound.

According to perturbation theory (Eckart 1948), the dependent fields f are decomposed as

$$f \approx f_0(\boldsymbol{r}, \tau) + f_1(\boldsymbol{r}, \tau, t_f) + f_2(\boldsymbol{r}, \tau), \tag{2.2}$$

where f_0 are zeroth-order (background) fields, f_1 are first-order time-harmonic acoustic fields $f_1 = f_a(\boldsymbol{r}, \tau)\,\mathrm{e}^{-\mathrm{i}\omega t_f}$, actuated at an angular frequency $\omega(\sim 1$ MHz), and f_2 are second-order fields (in general $f_2 \ll f_1$). In microscale flows, since the hydrostatic pressure $\rho g H(\sim 1$ Pa$) \ll p_1(\sim 10^6$ Pa), the variation of pressure and velocity fields due to gravity is accounted in the second-order effects. Thus, in a quiescent fluid, we take the zeroth-order velocity $\boldsymbol{v}_0 = 0$, and pressure $p_0 = \text{const.}(\nabla p_0 = 0)$.

The first-order acoustic fields vary on the fast time scale t_f ($t_f \sim 1/\omega \sim 0.1\ \mu$s), whereas the second-order hydrodynamic fields vary on the slow time scale τ ($\tau \gg t_f$). Usually in perturbation theory, $f_0(\boldsymbol{r}, \tau)$ is assumed to be constant for homogeneous fluids. Whereas for inhomogeneous fluids, the variation in the background fields (ρ_0, s_0, c_0 and η_0) with space as well as the slow time scale has to be accounted for due to the gravity stratification and second-order acoustic effects. As the first-order acoustic fields (f_1) are sensitive to the inhomogeneous configuration (ρ_0, s_0, c_0 and η_0) which varies on the slow time scale, the amplitude of these acoustic fields are considered to be a function of the slow time scale ($f_a(\boldsymbol{r}, \tau)$) unlike homogeneous fluids, where the amplitude of these fields is only a function of space ($f_a(\boldsymbol{r})$).

The variation of zeroth-order fields on the fast time scale (t_f) can be neglected. Also, since $D \sim O(10^{-9})$, the diffusion term is negligible on the fast time scale, due to which the composition of any given fluid particle remains unchanged as it moves. Consequently, the governing equations up to first order ($t \sim t_f$) reduce to (Bergmann 2005)

$$\partial_t\rho_1 + \nabla\cdot(\rho_0\boldsymbol{v}_1) = 0, \tag{2.3a}$$

$$\rho_0\partial_t\boldsymbol{v}_1 = -\nabla p_1 + \eta\nabla^2\boldsymbol{v}_1 + \beta\eta\nabla(\nabla\cdot\boldsymbol{v}_1), \tag{2.3b}$$

$$\partial_t s_1 + \boldsymbol{v}_1\cdot\nabla s_0 = 0, \tag{2.3c}$$

$$\partial_t\rho_1 + (\boldsymbol{v}_1\cdot\nabla)\rho_0 = (1/c^2)[\partial_t p_1]. \tag{2.3d}$$

The first-order fields have a harmonic time dependence, thus the time average of these fields is zero. Therefore, first-order terms in (2.3) cannot cause any bulk fluid motion. However, the N-S equation is nonlinear and the above linearized equations (2.3) are not exact. Hence, proceeding to solve (2.1) up to second order ($t \sim \tau$),

$$\langle\partial_t(\rho_0+\rho_2)\rangle + \nabla\cdot\langle\rho_1\boldsymbol{v}_1\rangle + \nabla\cdot\langle\rho_0\boldsymbol{v}_2\rangle = 0, \tag{2.4a}$$

$$\langle\rho_1\partial_t\boldsymbol{v}_1\rangle + \rho_0\langle(\boldsymbol{v}_1\cdot\nabla)\boldsymbol{v}_1\rangle - \langle(\rho_0+\rho_2)\boldsymbol{g}\rangle = -\nabla\langle p_2\rangle$$
$$+\eta\nabla^2\langle\boldsymbol{v}_2\rangle + \beta\eta\nabla(\nabla\cdot\langle\boldsymbol{v}_2\rangle) - \langle\rho_0\partial_t\boldsymbol{v}_2\rangle, \tag{2.4b}$$

$$\langle\partial_t(s_0+s_2)\rangle + \langle\boldsymbol{v}_2\cdot\nabla s_0\rangle + \langle\boldsymbol{v}_1\cdot\nabla s_1\rangle = D\nabla^2\langle(s_0+s_2)\rangle, \tag{2.4c}$$

$$\langle\partial_t(\rho_0+\rho_2)\rangle + \langle(\boldsymbol{v}_1\cdot\nabla)\rho_1\rangle + \langle(\boldsymbol{v}_2\cdot\nabla)\rho_0\rangle = (1/c^2)[\langle\partial_t p_2\rangle + \langle(\boldsymbol{v}_1\cdot\nabla)p_1\rangle], \tag{2.4d}$$

where $\langle\cdots\rangle$ denotes time average over one oscillation period. Since the time average of the product of two first-order fields is non-zero (the time average of two first-order fields

$\langle u_1 v_1 \rangle$ is defined as $\frac{1}{2}\text{Real}(u_1^\star v_1)$, where $\star$ denotes complex conjugation), they act as a source term for second-order fields (slow hydrodynamic time scale). The first two terms on the left side of (2.4*b*) together comprise the divergence of the Reynolds stress tensor, $\boldsymbol{\nabla} \cdot \langle \rho_0 \boldsymbol{v}_1 \otimes \boldsymbol{v}_1 \rangle = \boldsymbol{\nabla} \cdot \langle \rho_0 \boldsymbol{v}_1 \boldsymbol{v}_1 \rangle$.

In microscale flows, the variation of second-order fields with respect to the slow time scale is negligible (Bruus 2011; Friend & Yeo 2011). From (2.3), we get $\rho_1 \ll \rho_0$, $s_1 \ll s_0$ (see Appendix A) and from general perturbation theory, $f_2 \ll f_1$ (for any perturbed field f), thus $\rho_2 \ll \rho_0$ and $s_2 \ll s_0$. We can also neglect $\langle \boldsymbol{v}_1 \cdot \boldsymbol{\nabla} s_1 \rangle$, $\langle \rho_1 \boldsymbol{\nabla} \cdot \boldsymbol{v}_1 \rangle$ since the first-order fields in both these terms are out of phase (see Appendix A). Using the above arguments, combining ((2.4*a*) and (2.4*d*)),

$$\langle \rho_0 \boldsymbol{\nabla} \cdot \boldsymbol{v}_2 \rangle = -(1/c^2) \langle \boldsymbol{v}_1 \cdot \boldsymbol{\nabla} p_1 \rangle. \tag{2.5}$$

Substituting the above relation in (2.4*b*) and analysing the order of magnitude, $O(\beta \eta \boldsymbol{\nabla} (1/\rho_0 c_0^2)(\boldsymbol{v}_1 \cdot \boldsymbol{\nabla}) p_1) \ll O(\boldsymbol{\nabla} \cdot \langle \rho_0 \boldsymbol{v}_1 \boldsymbol{v}_1 \rangle)$. As this term, $(1/c^2)\langle \boldsymbol{v}_1 \cdot \boldsymbol{\nabla} p_1 \rangle$ does not contribute to the momentum equation, it does not affect the second-order velocity and pressure fields and thus can be neglected. Hence, (2.5) becomes divergence free and second-order flow is incompressible i.e. $\boldsymbol{\nabla} \cdot \langle \boldsymbol{v}_2 \rangle = 0$ (Nyborg's approximation; Nyborg 2005; Baasch, Doinikov & Dual 2020). Accounting for all the above arguments, the governing equations reduce to

$$\boldsymbol{\nabla} \cdot \langle \boldsymbol{v}_2 \rangle = 0, \tag{2.6a}$$

$$-\boldsymbol{\nabla} \cdot \langle \rho_0 \boldsymbol{v}_1 \boldsymbol{v}_1 \rangle + \langle \rho_0 \boldsymbol{g} \rangle - \boldsymbol{\nabla} \langle p_2 \rangle + \eta \boldsymbol{\nabla}^2 \langle \boldsymbol{v}_2 \rangle = 0, \tag{2.6b}$$

$$\langle \partial_t s_0 \rangle + \langle \boldsymbol{v}_2 \cdot \boldsymbol{\nabla} s_0 \rangle = D \boldsymbol{\nabla}^2 \langle s_0 \rangle. \tag{2.6c}$$

The above (2.6) govern the dynamics of inhomogeneous fluids in microscale acoustofluidics and can also be derived by another approach, see Appendix B. From (2.6*b*), it is evident that second-order slow hydrodynamic flows are created due to the divergence of the Reynolds stress tensor consisting of the product of first-order fast acoustic fields. Thus, we introduce the body force due to acoustic fields as

$$\boldsymbol{f}_{ac} = -\boldsymbol{\nabla} \cdot \langle \rho_0 \boldsymbol{v}_1 \boldsymbol{v}_1 \rangle. \tag{2.7}$$

It is well known that the above force is responsible for boundary-driven Rayleigh streaming and bulk-driven Eckart streaming in homogeneous fluids. In this work, we proceed to show that the same force is also responsible for recently observed streaming suppression and acoustic relocation of miscible as well as immiscible inhomogeneous fluids. A microchannel of width $w = 380$ μm and height $h = 160$ μm is chosen for study from Muller & Bruus (2014) containing an inhomogeneous miscible solution, as shown in figure 1. Fluid properties are taken from Qiu *et al.* (2019). An acoustic standing half-wave along the width is imposed in the microchannel by actuating both the sidewalls in phase at a specific frequency 'ν' and wall displacement 'd' in the x-direction. The first-order fields due to this standing wave are obtained by solving (2.3) in the frequency domain, see Appendix C. These first-order fields are then used to obtain the acoustic body force (2.7) to solve the time-averaged second-order fields (2.6). At each time step, the first-order fields are solved for the updated inhomogeneous fluid configuration (ρ_0, c_0, η_0) from the previous time step. Hence, both the first-order and second-order equations are bidirectionally coupled and solved numerically at all slow time steps in COMSOL Multiphysics 5.6. The mesh convergence for the numerical simulation is discussed in Appendix G.

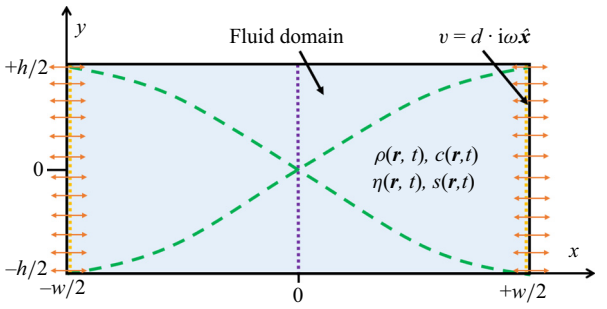

Figure 1. Sketch of acoustofluidic microchannel with an imposed half-wave acoustic pressure resonance, containing fluids whose density, speed of sound, dynamic viscosity and solute concentration are functions of space and time.

3. Results and discussion

From figure 2, the acoustic body force $\boldsymbol{f}_{ac}$ tends to relocate high impedance fluid to nodes and low impedance to anti-nodes, called a stable configuration (whereas any other configuration with an impedance gradient is considered unstable). Once the stable configuration is reached, due to the existing impedance gradient, this $\boldsymbol{f}_{ac}$ inhibits any fluid motion due to gravity and suppresses acoustic streaming, which tries to disturb the stable configuration, as seen in figures 2 and 3. As time progresses, due to diffusion, the fluid profile becomes homogeneous, where the same $\boldsymbol{f}_{ac}$ induces boundary-driven Rayleigh streaming. From these results, it is evident that the acoustic body force $\boldsymbol{f}_{ac}$ is responsible for acoustic relocation and streaming suppression in inhomogeneous fluids as well as acoustic streaming in homogeneous fluids. Remarkably, in the process of acoustic relocation and diffusion, as shown in figures 2(a) and 3(a), the amplitude of the first-order fields (p_a and v_a) varies significantly (see Appendix D) as the background ρ_0 and c_0 fields change on the slow time scale. Thus, the acoustic energy density E_{ac}, which is a function of p_a, ρ_0 and c_0, also changes significantly, in contrast to constant E_{ac} assumed in previous studies (Karlsen *et al.* 2016; Karlsen 2018; Karlsen *et al.* 2018). Surprisingly, it is observed that, for the case of constant impedance (figure 4), relocation does not occur irrespective of the ρ_0 and c_0 configurations, thus any constant impedance configuration is called a neutral configuration. This demonstrates that the impedance gradient is the requisite and governing factor for acoustic relocation. In addition to the impedance gradient being a prerequisite, the sufficient conditions for acoustic relocation include: the fluid interface should not be at a node (See Appendix E) and the fluid configuration must be unstable.

In order to explain the above results mathematically, we analyse the acoustic body force, $\boldsymbol{f}_{ac} = -\boldsymbol{\nabla}\cdot\langle\rho_0\boldsymbol{v}_1\boldsymbol{v}_1\rangle$ in detail

$$\boldsymbol{f}_{ac} = \boldsymbol{\nabla}\cdot\langle\rho_0\boldsymbol{v}_1\otimes\boldsymbol{v}_1\rangle = -\boldsymbol{\nabla}\cdot\langle\rho_0\boldsymbol{v}_1\boldsymbol{v}_1\rangle = -\rho_0\langle\boldsymbol{v}_1\cdot\boldsymbol{\nabla}\boldsymbol{v}_1\rangle - \langle\rho_1\partial_t\boldsymbol{v}_1\rangle. \tag{3.1}$$

Using the following identity $\boldsymbol{A}\cdot\boldsymbol{\nabla}\boldsymbol{A} = \boldsymbol{\nabla}(\boldsymbol{A}^2/2) - \boldsymbol{A}\times(\boldsymbol{\nabla}\times\boldsymbol{A})$ and substituting first-order fields from (2.3), (3.1) becomes

$$\begin{aligned}\boldsymbol{f}_{ac} = &-\frac{1}{2\rho_0}\boldsymbol{\nabla}\langle|\rho_0\boldsymbol{v}_1|^2\rangle + \langle\boldsymbol{v}_1\times\boldsymbol{\nabla}\times(\rho_0\boldsymbol{v}_1)\rangle + \frac{1}{2}\kappa_0\boldsymbol{\nabla}\langle|p_1|^2\rangle\\ &- \langle(\kappa_0 p_1)(\eta\nabla^2\boldsymbol{v}_1 + \beta\eta\boldsymbol{\nabla}(\boldsymbol{\nabla}\cdot\boldsymbol{v}_1))\rangle.\end{aligned} \tag{3.2}$$

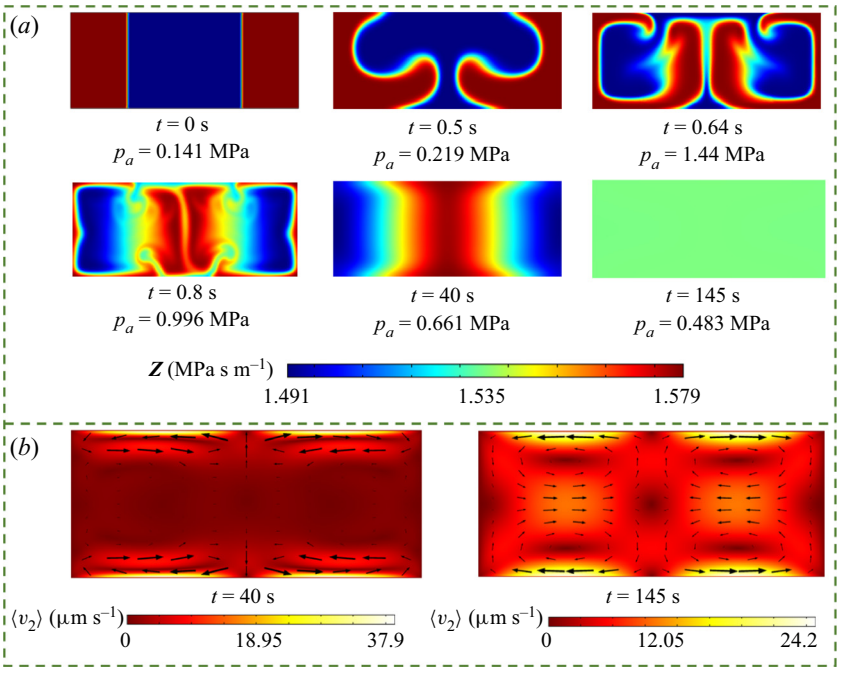

Figure 2. (*a*) Relocation of unstable configuration to stable configuration with $d = 0.261$ nm and $\nu = 1.96$ MHz. Initially ($t = 0$ s), there is low impedance deionized (DI) water (blue) at the centre and high impedance 10 % Ficoll PM70 (red) at the sides. The green image indicates the homogeneous fluid profile after relocation and complete diffusion. (*b*) Second-order velocity $\langle \boldsymbol{v}_2 \rangle$.

For a detailed derivation refer to Appendix F. From the scaling analysis, the last term in (3.2) can be neglected, thus reducing to

$$\boldsymbol{f}_{ac} = \tfrac{1}{2}\nabla(\kappa_0\langle|p_1|^2\rangle - \rho_0\langle|\boldsymbol{v}_1|^2\rangle) + \langle \boldsymbol{v}_1 \times \nabla \times (\rho_0 \boldsymbol{v}_1)\rangle - \tfrac{1}{2}[\langle|p_1|^2\rangle\nabla\kappa_0 + \langle|\boldsymbol{v}_1|^2\rangle\nabla\rho_0]. \tag{3.3}$$

In the above (3.3), the first term $(1/2)\nabla(\kappa_0\langle|p_1|^2\rangle - \rho_0\langle|\boldsymbol{v}_1|^2\rangle)$ is a pure gradient term (conservative), and the curl of that term is zero, thus it does not cause relocation or streaming but only contributes to the second-order pressure. The third term $(-1/2)[\langle|p_1|^2\rangle\nabla\kappa_0 + \langle|\boldsymbol{v}_1|^2\rangle\nabla\rho_0]$ is responsible for relocation, since the curl of this term, in general, is non-zero. From (2.3*b*), the first-order fields in the inviscid region satisfy the following relation, $\nabla \times (\rho_0 \boldsymbol{v}_1) = 0$. Thus the second term $\langle \boldsymbol{v}_1 \times \nabla \times (\rho_0 \boldsymbol{v}_1)\rangle$ is only significant inside the boundary layer ($\delta \sim 1$ μm) of first-order fields, which is responsible for boundary-driven streaming in inhomogeneous fluids. The competition between the relocation force (third term) and streaming force (second term) accounts for streaming suppression, as seen in figures 2 and 3. In (3.3), we have analytically separated relocation and streaming causing terms from the general body force term, $\boldsymbol{f}_{ac}$, which was previously claimed not to be possible by Karlsen *et al.* (2018). For homogeneous fluids (3.3) reduces to (Bradley 1998; Friend & Yeo 2011)

$$\boldsymbol{f}_{ac} = -\nabla \cdot \langle \rho_0 \boldsymbol{v}_1 \boldsymbol{v}_1 \rangle = \tfrac{1}{2}(\kappa_0 \nabla\langle|p_1|^2\rangle - \rho_0 \nabla\langle|\boldsymbol{v}_1|^2\rangle) + \{\rho_0\langle \boldsymbol{v}_1 \times (\nabla \times \boldsymbol{v}_1)\rangle\}, \tag{3.4}$$

where the first term is the homogeneous second-order mean Eulerian pressure and the second term is responsible for acoustic streaming.

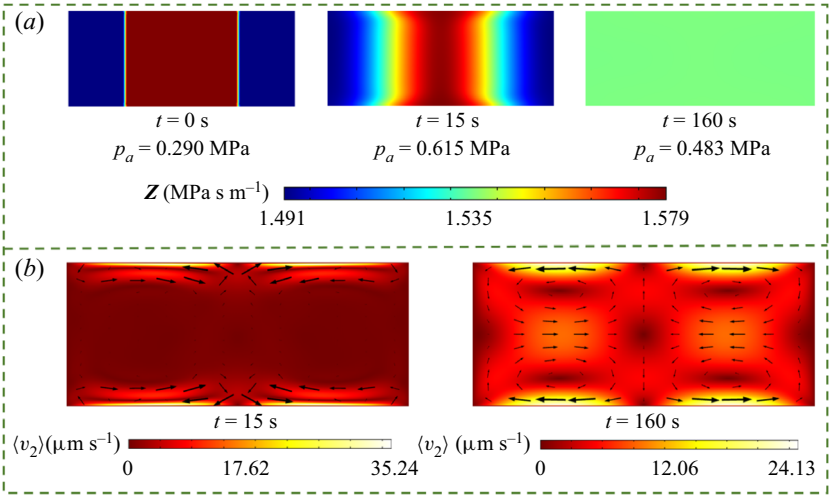

Figure 3. (*a*) Stable configuration with no relocation, with low impedance DI water (blue) at the sides and high impedance 10 % Ficoll PM70 (red) at the centre. The green image indicates the homogeneous fluid profile after complete diffusion. (*b*) Second-order velocity $\langle \boldsymbol{v}_2 \rangle$. Here, $d = 0.261$ nm and $\nu = 1.96$ MHz. Relocation force ($\boldsymbol{f}_{rl}$) stabilizes this configuration against gravitational stratification.

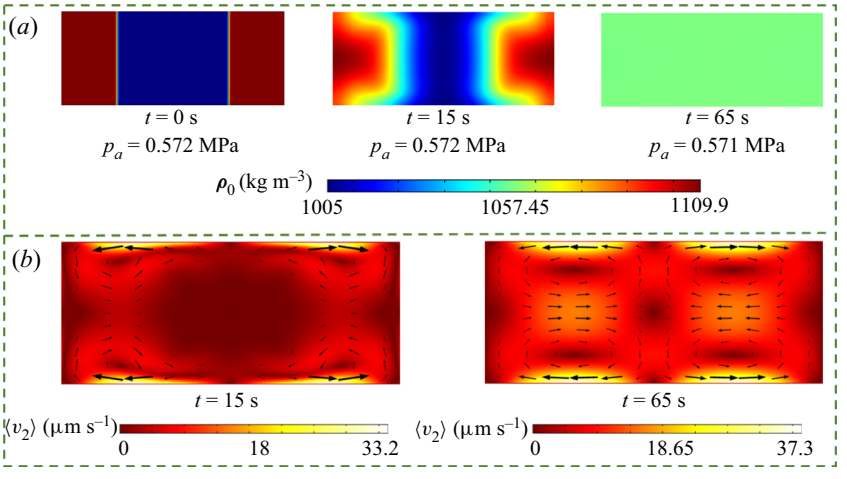

Figure 4. For constant impedance fluids any configuration of ρ_0 and c_0 is a neutral configuration. (*a*) No relocation due to zero relocation force ($\boldsymbol{f}_{rl} = 0$). To clearly show the absence of a relocation force in the constant impedance case, gravity is neglected. The presence of gravity would stratify the fluids. The green image indicates the homogeneous fluid profile after complete diffusion. (*b*) Second-order velocity $\langle \boldsymbol{v}_2 \rangle$. Here, $d = 2$ nm and $\nu = 1.96$ MHz.

To understand the second-order pressure and relocation phenomenon in inhomogeneous fluids clearly, we study the acoustic body force outside the boundary layer of first-order fields (neglecting the streaming term). Thus, (3.3), after time averaging, reduces to

$$\begin{aligned} \boldsymbol{f}_{ac} &= -\boldsymbol{\nabla} \cdot \langle \rho_0 \boldsymbol{v}_1 \boldsymbol{v}_1 \rangle = \tfrac{1}{4}\boldsymbol{\nabla}(\kappa_0 |p_1|^2 - \rho_0 |\boldsymbol{v}_1|^2)[-\tfrac{1}{4}|p_1|^2 \boldsymbol{\nabla}\kappa_0 - \tfrac{1}{4}|\boldsymbol{v}_1|^2 \boldsymbol{\nabla}\rho_0] \\ &= \boldsymbol{f}_1 + [\boldsymbol{f}_2]. \end{aligned} \tag{3.5}$$

Considering the case of a stable configuration (figure 3), the second-order velocity will be zero as relocation does not take place due to which (2.6*b*) will reduce to $-\boldsymbol{\nabla}\cdot\langle\rho_0\boldsymbol{v}_1\boldsymbol{v}_1\rangle = \boldsymbol{\nabla}\langle p_2\rangle$. Now, it is evident that, in the inviscid case, both the terms ($\boldsymbol{f}_1$,$\boldsymbol{f}_2$) in (3.5) contribute to the mean Eulerian pressure $\langle p_2\rangle$, whereas, in Karlsen *et al.* (2016), Karlsen (2018) and Karlsen *et al.* (2018), it is hypothesized that only the first term in (3.5) contributes to the mean Eulerian pressure, $\langle p_2\rangle = \frac{1}{2}\kappa_0\langle|p_1|^2\rangle - \frac{1}{2}\rho_0\langle|\boldsymbol{v}_1|^2\rangle$. Thus, our work clearly demonstrates that $\langle p_2\rangle$ can be derived from the governing equations and their assumption on $\langle p_2\rangle$ is incorrect and needless.

In the case of constant impedance ($Z_0 = \rho_0 c_0 = \text{const.}$) inhomogeneous fluids, subjected to a one-dimensional acoustic standing half-wave ($\lambda \approx 2w$), using the relations $p_1 = p_a\sin(kx)$ and $v_1 = (p_a/i\rho_0 c_0)\cos(kx)$ where $k = 2\pi/\lambda$ is wavenumber, the relocation force term $\boldsymbol{f}_2$ reduces to

$$\boldsymbol{f}_{2|Z=C} = -\frac{1}{4}|p_1|^2\boldsymbol{\nabla}\kappa_0 - \frac{1}{4}|\boldsymbol{v}_1|^2\boldsymbol{\nabla}\rho_0 = -\boldsymbol{\nabla}\left(\frac{p_a^2\rho_0}{4Z^2}\right). \tag{3.6}$$

Since $\boldsymbol{f}_2$ reduces to a purely gradient term in the case of constant impedance inhomogeneous fluids, it does not induce relocation or motion but only contributes to the second-order pressure. Thus, we prove that the impedance gradient is the necessary condition for acoustic relocation, which agrees with experimental results (Deshmukh *et al.* 2014; Hemachandran *et al.* 2019).

For the case of variable impedance, the relocation term $\boldsymbol{f}_2$ in (3.5) is written as

$$\boldsymbol{f}_2 = \frac{p_a^2\sin^2(kx)}{4}\left(\frac{\boldsymbol{\nabla}\rho_0}{\rho_0^2c_0^2}\right) + \frac{p_a^2\sin^2(kx)}{2}\left(\frac{\boldsymbol{\nabla}c_0}{\rho_0c_0^3}\right) - \frac{p_a^2\cos^2(kx)}{4}\left(\frac{\boldsymbol{\nabla}\rho_0}{\rho_0^2c_0^2}\right), \tag{3.7}$$

$$\boldsymbol{f}_2 = -\frac{p_a^2\cos(2kx)}{4\rho_0^2c_0^3}\boldsymbol{\nabla}Z_0 + \frac{p_a^2}{4\rho_0c_0^3}\boldsymbol{\nabla}c_0. \tag{3.8}$$

Analogous to the Boussinesq approximation, $\boldsymbol{\nabla}Z_0/\rho_0^2c_0^3 \approx \boldsymbol{\nabla}Z_0/\rho_{avg}^2c_{avg}^3$, $\boldsymbol{\nabla}c_0/\rho_0c_0^3 \approx \boldsymbol{\nabla}c_0/\rho_{avg}c_{avg}^3$ and substituting (3.8) in (3.5), separating gradient and non-gradient terms,

$$\begin{aligned}\boldsymbol{f}_{ac} = -\boldsymbol{\nabla}\cdot\langle\rho_0\boldsymbol{v}_1\boldsymbol{v}_1\rangle &= -E_{ac}\cos(2kx)\boldsymbol{\nabla}\hat{Z}_0\\ &\quad - \boldsymbol{\nabla}(\tfrac{1}{4}\rho_0|\boldsymbol{v}_1|^2 - \tfrac{1}{4}\kappa_0|p_1|^2 - E_{ac}\hat{c}_0),\end{aligned} \tag{3.9}$$

where $E_{ac} = p_a^2/(4\rho_{avg}c_{avg}^2)$, $\hat{c}_0 = c_0/c_{avg}$, $\hat{\rho}_0 = \rho_0/\rho_{avg}$ and $\hat{Z}_0 = \hat{\rho}_0\hat{c}_0$.

It is clear that only the first term in (3.9) is responsible for acoustic relocation in inhomogeneous fluids, whereas the second term resembles a conservative or purely gradient term, thus inducing only pressure. Thus, in addition to the impedance gradient being the necessary factor for relocation, now we write the relocation force in terms of the impedance gradient as follows:

$$\boldsymbol{f}_{rl} = -E_{ac}\cos(2kx)\boldsymbol{\nabla}\hat{Z}_0. \tag{3.10}$$

The above force term, which is a part of the generalized force (2.7), is responsible for the relocation of the unstable configuration in figure 2 and maintaining the stable configuration by inhibiting acoustic streaming as well as gravity stratification in figure 3. Whereas, for constant impedance fluids (figure 4), irrespective of any fluid configuration, the relocation force is always absent ($\boldsymbol{f}_{rl} = 0$).

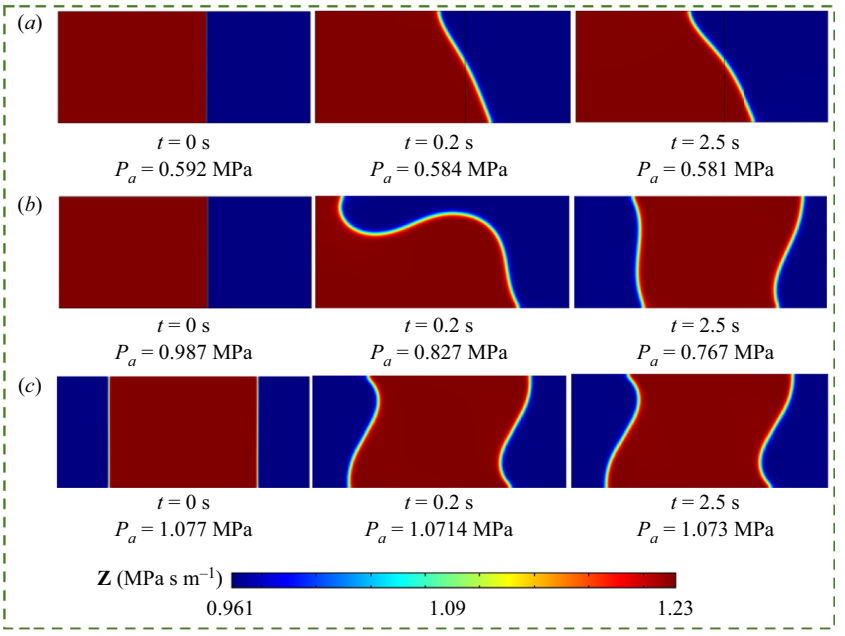

Figure 5. Relocation of immiscible fluids by actuating all walls of a microchannel (two-dimensional), consisting of high impedance mineral oil (red) and low impedance silicone oil (blue) with a surface tension of 1 mN m^{-1} actuated at a frequency of 2.1 MHz for unstable configurations. (*a*) No relocation for $E_{ac} < E_{cr}$, slight fluid displacement is attributed to slanted node alignment. (*b*) Relocation for $E_{ac} > E_{cr}$. (*c*) Stable configuration, no relocation for any E_{ac}, slight fluid displacement is attributed to slanted node alignment.

In several previous studies (Karlsen & Bruus 2017; Nath & Sen 2019; Qiu *et al.* 2019), including ours (Pothuri, Azharudeen & Subramani 2019; Kumar *et al.* 2021), (3.8) has been used to study relocation without realizing that it contains implicit gradient or conservative terms which do not contribute to relocation. This leads to an incorrect scaling analysis and thus it is necessary to ignore this gradient term in such circumstances. Furthermore, (3.10) captures all the aspects of relocation and does not cause scaling issues like (3.8). It must be noted that (3.10) is valid only outside the boundary layer of first-order fields, whereas inside the boundary layer, it cannot be reduced from $\boldsymbol{f}_2$ of (3.5). This is because $p_1 = p_a \sin(kx)$ remains the same inside and outside the boundary layer ($\delta \sim 1\ \mu$m), but $v_1 \neq (p_a/i\rho_0 c_0)\cos(kx)$ and $\partial_y v_1$ is significant inside the boundary layer due to the no-slip condition. Thus, in the case of constant impedance fluids, the relocation force is absent in the bulk but non-zero within the boundary layer, which is responsible for the disturbance of homogeneous streaming, as in figure 4.

Immiscible fluids. The phenomenon of acoustic relocation of immiscible fluids due to a standing acoustic wave is also governed by (2.7). This theory predicts that, for the relocation of immiscible fluids to occur, the applied acoustic energy density E_{ac} must be greater than the threshold E_{cr} to overcome the interfacial tension force. The above prediction is in agreement with the experimental studies by Hemachandran *et al.* (2019). However, in their study, relocation is achieved irrespective of the interface location with respect to the node. Also, the frequency employed is very different from the resonant frequency ($\nu = c_{avg}/2w$) that corresponds to the standing half-wave actuated only along the width of the microchannel, as shown in figure 1. Contrary to their study, when we actuated only sidewalls, relocation seemed to be highly dependent on the position of

the interface and was absent when the interface and node coincide. Whereas, when all the walls were actuated in the direction of their surface normal, we achieved relocation, independent of the interface location, (figure 5), which is in agreement with their experiments (Hemachandran *et al.* 2019). It is evident that relocation can be achieved through two modes; one is due to a one-dimensional standing wave resulting from the actuation of the sidewalls at the one-dimensional resonant frequency ($\nu = c_{avg}/2w$) while the other is due to a two-dimensional standing wave resulting from the actuation of all walls at the two-dimensional resonant frequency (between $\nu = c_{avg}/2w$ and $\nu = c_{avg}/2h$). Since the relocation in Hemachandran *et al.* (2019) is due to a two-dimensional standing wave, the frequency required (∼2.1–2.4 MHz) for relocation (for silicone–mineral oil) is different from the one-dimensional resonant frequency (1.66 MHz). The velocity and pressure fields of the relocation of immiscible fluids due to a two-dimensional standing wave are shown in Appendix E.

4. Conclusion

We have put forward a theory of nonlinear acoustics that governs the acoustic phenomena of relocation and streaming suppression in inhomogeneous miscible and immiscible fluids (including streaming in homogeneous fluids). This theory also confirms the fact that the divergence of the time-averaged Reynolds tensor $-\boldsymbol{\nabla} \cdot \langle \rho_0 \boldsymbol{v}_1 \boldsymbol{v}_1 \rangle$ is alone responsible for all the above processes. We showed that first-order fields p_1, $\boldsymbol{v}_1$ and energy density E_{ac} vary significantly during the process of acoustic relocation and diffusion. Importantly, we have proved that an impedance gradient is the necessary condition for relocation. The other conditions for acoustic relocation in one- and two-dimensional modes will be addressed in detail using stability analysis for both miscible and immiscible fluids in an upcoming paper. The fundamental understanding from this study can give new insights into particle (cells/drops/beads) and inhomogeneous fluid handling in microchannels under acoustic fields.

Funding. This work is supported by IIITDM Kancheepuram via Grant No: IRG/2019-20/KS/006.

Declaration of interests. The authors report no conflict of interest.

Author ORCIDs.
Karthick Subramani https://orcid.org/0000-0002-7751-7759.

Appendix A. Order of magnitude analysis

The order of magnitude analysis for different terms considered at various steps in the derivations is given below. The proof of the stated assumption $\rho_1 \ll \rho_0$ and $s_1 \ll s_0$ is as follows. We shall first obtain the order for $\boldsymbol{v}_1$ from (2.3*b*). The viscous effects are dominant only inside the thin viscous boundary layer (∼ 1 μm), due to which we can take only the first term, i.e. $\rho_0 \partial_t \boldsymbol{v}_1$, which has an effect on the entire medium. Thus comparing its magnitude with $\boldsymbol{\nabla} p_1$, we get

$$O(\rho_0 \partial_t \boldsymbol{v}_1) \sim O(\boldsymbol{\nabla} p_1). \tag{A1}$$

It is known that the first-order pressure (p_1) in the domain in our study is of the order of $\sim 10^6$, $\rho_0 \sim O(10^3)$, wavenumber $k \sim O(10^4)$ and $\omega \sim O(10^6)$ (the time derivative can

be written in terms of the angular frequency as $-\mathrm{i}\omega$, where i represents a complex root)

$$\boldsymbol{v}_1 \sim \frac{kp_1}{\rho_0\,\mathrm{i}\omega} \sim \frac{1}{0.76} \sim 1. \tag{A2}$$

In the above simplification, wavelength λ is considered as 760 μm (it is chosen as twice the width of the channel in order to get a one-dimensional half-standing wave along this dimension of the channel). Using this order of $\boldsymbol{v}_1$ in ((2.3*c*) and (2.3*d*)), we have

$$s_1 \sim \frac{\boldsymbol{v}_1 k s_0}{\mathrm{i}\omega} \sim 10^{-2}(s_0), \tag{A3a}$$

$$\rho_1 \sim \frac{\boldsymbol{v}_1 k \rho_0}{\mathrm{i}\omega} \sim 10^{-4}(\rho_0). \tag{A3b}$$

Thus, it is conclusive that $s_1 \ll s_0$ and $\rho_1 \ll \rho_0$.

On simplifying to the second-order equations, we have stated that $O(\beta\eta\nabla(1/\rho_0 c_0^2)\langle(\boldsymbol{v}_1\cdot\nabla)p_1\rangle) \ll O(\nabla\cdot\langle\rho_0\boldsymbol{v}_1\boldsymbol{v}_1\rangle)$ and the proof for this follows. Using the order of magnitudes as $\beta \sim O(10^{-1})$, $\eta \sim O(10^{-3})$, $\delta \sim O(10^{-6})$, $c \sim O(10^3)$ and the magnitudes for other variables as considered above, we have

$$\beta\eta\nabla\left(\frac{1}{\rho_0 c_0^2}\langle(\boldsymbol{v}_1\cdot\nabla)p_1\rangle\right) \sim \frac{\beta\eta}{\delta}\left(\frac{1}{\rho_0 c_0^2}(\boldsymbol{v}_1 k)p_1\right) \sim \frac{10^{-1}10^{-3}}{10^{-6}}\left(\frac{10^4 10^6}{10^9}\right) \sim 10^3, \tag{A4a}$$

$$\nabla\cdot\langle\rho_0\boldsymbol{v}_1\boldsymbol{v}_1\rangle \sim k\rho_0\boldsymbol{v}_1\boldsymbol{v}_1 \sim 10^4 10^3 \sim 10^7. \tag{A4b}$$

Thus, $\beta\eta\nabla(1/\rho_0 c_0^2)\langle(\boldsymbol{v}_1\cdot\nabla)p_1\rangle$ is 10^4 orders less than $\nabla\cdot\langle\rho_0\boldsymbol{v}_1\boldsymbol{v}_1\rangle$.

We have also stated that the first-order fields in the terms $\langle\boldsymbol{v}_1\cdot\nabla s_1\rangle$, $\langle\rho_1\nabla\cdot\boldsymbol{v}_1\rangle$ are out of phase. The below is the proof for this. From (C1*a*) and $\boldsymbol{v}_1 = \boldsymbol{v}_a(r,\tau))\,\mathrm{e}^{-\mathrm{i}\omega t_f}$ (first-order time-harmonic acoustic field), we have

$$-\mathrm{i}\omega\rho_1 = \nabla\cdot(\rho_0\boldsymbol{v}_1) = \nabla\cdot(\rho_0\boldsymbol{v}_a(r,\tau))\,\mathrm{e}^{-\mathrm{i}\omega t_f}, \tag{A5a}$$

$$\rho_1 = Re\left[\frac{\mathrm{i}\nabla\cdot(\rho_0\boldsymbol{v}_a(r,\tau))\,\mathrm{e}^{-\mathrm{i}\omega t_f}}{\omega}\right], \tag{A5b}$$

where $\boldsymbol{v}_a$ is the velocity amplitude. The complex 'i' in the ρ_1 expression indicates a phase shift between the velocity and density oscillations. Thus, ρ_1 and $\boldsymbol{v}_1$ are out of phase (Muller & Bruus 2014). Similarly, from (C1*c*), we have

$$-\mathrm{i}\omega s_1 = -\boldsymbol{v}_1\cdot\nabla s_0 = -\boldsymbol{v}_a(r,\tau)\,\mathrm{e}^{-\mathrm{i}\omega t_f}\cdot\nabla s_0, \tag{A6a}$$

$$s_1 = Re\left[\frac{-\mathrm{i}\boldsymbol{v}_a(r,\tau)\,\mathrm{e}^{-\mathrm{i}\omega t_f}\cdot\nabla s_0}{\omega}\right]. \tag{A6b}$$

Thus $\boldsymbol{v}_1$ and s_1 are out of phase.

Appendix B. Derivation of governing equations for inhomogeneous fluids – alternate approach

The hydrodynamics of inhomogeneous fluids considered in this study is governed by the mass continuity, momentum and advection–diffusion equations, which are given below

$$\partial_t \rho + \boldsymbol{\nabla} \cdot (\rho \boldsymbol{v}) = 0, \tag{B1a}$$

$$\rho[\partial_t \boldsymbol{v} + (\boldsymbol{v} \cdot \boldsymbol{\nabla})\boldsymbol{v}] = -\boldsymbol{\nabla} p + \eta \nabla^2 \boldsymbol{v} + \beta \eta \boldsymbol{\nabla}(\boldsymbol{\nabla} \cdot \boldsymbol{v}) + \rho \boldsymbol{g}, \tag{B1b}$$

$$\partial_t s + \boldsymbol{v} \cdot \boldsymbol{\nabla} s = D \nabla^2 s, \tag{B1c}$$

where ρ is the density, $\boldsymbol{v}$ is the velocity, p is the pressure, η is the dynamic viscosity of the fluid, ξ is the volume fluid viscosity, $\beta = (\xi/\eta) + (1/3)$, s is the solute concentration and D is the diffusivity. When the fluid is subjected to acoustic waves, the following thermodynamic pressure density relation is required,

$$\frac{\mathrm{d}\rho}{\mathrm{d}t} = \frac{1}{c^2}\frac{\mathrm{d}p}{\mathrm{d}t}. \tag{B1d}$$

Say the fields are decomposed based on their variation on different time scales

$$f = f_0(\boldsymbol{r}, \tau) + f_1(\boldsymbol{r}, \tau)\, \mathrm{e}^{-\mathrm{i}\omega t_f}, \tag{B2}$$

where f_0 varies due to gravity and nonlinear effects on the slow time scale and f_1 varies on the fast time scale. The time scale of acoustics is of the order of microseconds ($t_f \sim 1/\omega \sim 0.1\ \mu\mathrm{s}$), whereas the hydrodynamic time scale of the order of milliseconds ($t_f \ll \tau$).

Substituting (B2) in the governing equations, we have

$$\partial_t(\rho_0 + \rho_1) + \boldsymbol{\nabla} \cdot [(\rho_0 + \rho_1)(\boldsymbol{v}_0 + \boldsymbol{v}_1)] = 0, \tag{B3a}$$

$$\begin{aligned}(\rho_0 + \rho_1)\partial_t(\boldsymbol{v}_0 + \boldsymbol{v}_1) + (\rho_0 + \rho_1)((\boldsymbol{v}_0 + \boldsymbol{v}_1) \cdot \boldsymbol{\nabla})(\boldsymbol{v}_0 + \boldsymbol{v}_1) \\ = -\boldsymbol{\nabla}(p_0 + p_1) + \eta \nabla^2(\boldsymbol{v}_0 + \boldsymbol{v}_1) + \beta \eta \boldsymbol{\nabla}(\boldsymbol{\nabla} \cdot (\boldsymbol{v}_0 + \boldsymbol{v}_1)) + (\rho_0 + \rho_1) g,\end{aligned} \tag{B3b}$$

$$\partial_t(s_0 + s_1) + (\boldsymbol{v}_0 + \boldsymbol{v}_1) \cdot \boldsymbol{\nabla}(s_0 + s_1) = D \nabla^2(s_0 + s_1), \tag{B3c}$$

$$\partial_t(\rho_0 + \rho_1) + ((\boldsymbol{v}_0 + \boldsymbol{v}_1) \cdot \boldsymbol{\nabla})(\rho_0 + \rho_1) = (1/c^2)[\partial_t(p_0 + p_1)]. \tag{B3d}$$

It is important to mention here that the pressure field on the slow time scale is decomposed as, $p_0 = p_c + p_g + p_s$, where p_c is the reference pressure, p_g is the pressure due to gravity and p_s is the second-order mean Eulerian pressure. Neglecting the influence of gravity and accounting for the fact that the reference pressure remains constant, the variation in p_0 is only due to the variation in p_s.

Before we proceed to the fast time scale equations, we propose the validity of this theory, i.e. it holds good only when $\boldsymbol{v}_0 \ll \boldsymbol{v}_1$ and $\boldsymbol{\nabla} p_0 \ll \boldsymbol{\nabla} p_1$, which is true in our case. On the fast time scale (t_f), the variation of the f_0 fields with respect to time can be neglected and since $D \sim O(10^{-9})$, the diffusion term is negligible, due to which the composition of any given fluid particle will remain unchanged as it moves. Also, from (B3*c*) and (B3*d*), it is evident that $s_1 \ll s_0$ and $\rho_1 \ll \rho_0$. Accounting for all the above arguments, the fast time

scale equations reduce to

$$\partial_t \rho_1 + \boldsymbol{\nabla} \cdot (\rho_0 \boldsymbol{v}_1) = 0, \tag{B4a}$$

$$\rho_0 \partial_t \boldsymbol{v}_1 = -\boldsymbol{\nabla} p_1 + \eta \nabla^2 \boldsymbol{v}_1 + \beta \eta \boldsymbol{\nabla}(\boldsymbol{\nabla} \cdot \boldsymbol{v}_1), \tag{B4b}$$

$$\partial_t s_1 + \boldsymbol{v}_1 \cdot \boldsymbol{\nabla} s_0 = 0, \tag{B4c}$$

$$\partial_t \rho_1 + \boldsymbol{v}_1 \cdot \boldsymbol{\nabla} \rho_0 = (1/c^2)[\partial_t p_1]. \tag{B4d}$$

However, the time average of these f_0 fields over one complete oscillation is zero, thus these fields cannot cause any bulk fluid motion. But the N-S equation is nonlinear and the above linearized equation is not exact. Thus, we must proceed to solve the fields on the slow time scale, which is responsible for the nonlinear effects. Since $\rho_1 \ll \rho_0$ and $\boldsymbol{v}_0 \ll \boldsymbol{v}_1$, the fast time-averaged, slow time scale equations reduce to

$$\langle \partial_t \rho_0 \rangle + \boldsymbol{\nabla} \cdot \langle \rho_0 \boldsymbol{v}_0 + \rho_1 \boldsymbol{v}_1 \rangle = 0, \tag{B5a}$$

$$\rho_0 \langle \partial_t \boldsymbol{v}_0 \rangle + \rho_1 \langle \partial_t \boldsymbol{v}_1 \rangle + \rho_0 \langle (\boldsymbol{v}_1 \cdot \boldsymbol{\nabla}) \boldsymbol{v}_1 \rangle = -\boldsymbol{\nabla} \langle p_0 \rangle + \eta \nabla^2 \langle \boldsymbol{v}_0 \rangle + \beta \eta \boldsymbol{\nabla}(\boldsymbol{\nabla} \cdot \langle \boldsymbol{v}_0 \rangle) + \rho_0 g, \tag{B5b}$$

$$\langle \partial_t s_0 \rangle + \langle \boldsymbol{v}_0 \cdot \boldsymbol{\nabla} s_0 \rangle + \langle \boldsymbol{v}_1 \cdot \boldsymbol{\nabla} s_1 \rangle = D \nabla^2 \langle s_0 \rangle, \tag{B5c}$$

$$\langle \partial_t \rho_0 \rangle + \langle \boldsymbol{v}_0 \cdot \boldsymbol{\nabla} \rho_0 \rangle + \langle \boldsymbol{v}_1 \cdot \boldsymbol{\nabla} \rho_1 \rangle = (1/c^2) \langle \boldsymbol{v}_1 \cdot \boldsymbol{\nabla} p_1 \rangle, \tag{B5d}$$

where $\langle \cdots \rangle$ denotes the time average for one oscillation period. From (B5*b*), it can be seen that the product of the fast time scale varying fields along with gravity act as source terms responsible for second-order fields, which cause a change in the fluid profile, due to which the amplitudes of fast scale fields also change accordingly at all time instants on the slow scale. Also, in inhomogeneous fluids, changing the background velocity field v_0, results in variation of ρ_0 and s_0 with respect to the slow time scale ($t \sim \tau$), thus $\langle \partial_t \rho_0 \rangle \neq 0$ and $\langle \partial_t s_0 \rangle \neq 0$. Along with $\rho_1 g \ll \rho_0 g$, $D \boldsymbol{\nabla} s_1 \ll D \boldsymbol{\nabla} s_0$, we also neglect $\langle \boldsymbol{v}_1 \cdot \boldsymbol{\nabla} s_1 \rangle$, $\langle \rho_1 \boldsymbol{\nabla} \cdot \boldsymbol{v}_1 \rangle$ since both these terms are out of phase. Using the above arguments, combining equations (B5*a*) and (B5*d*) we get

$$\langle \rho_0 \boldsymbol{\nabla} \cdot \boldsymbol{v}_1 \rangle = -(1/c^2) \langle \boldsymbol{v}_1 \cdot \boldsymbol{\nabla} p_1 \rangle. \tag{B6}$$

Substituting the above equation in (B6), since $\beta \eta \boldsymbol{\nabla}(1/\rho_0 c^2)(\boldsymbol{v}_1 \cdot \boldsymbol{\nabla}) p_1 \sim O(10^3) \ll \boldsymbol{\nabla} \cdot \langle \rho_0 \boldsymbol{v}_1 \boldsymbol{v}_1 \rangle \sim O(10^7)$ we can neglect the term $\beta \eta \boldsymbol{\nabla}(\boldsymbol{\nabla} \cdot \langle \boldsymbol{v}_1 \rangle)$. The term $(1/c^2) \langle \boldsymbol{v}_1 \cdot \boldsymbol{\nabla} p_1 \rangle$ does not contribute to any acoustic phenomena and can be neglected, thus we have $\boldsymbol{\nabla} \cdot \langle \boldsymbol{v}_1 \rangle = 0$, which indicates the flow is incompressible. This is stated as Nyborg's divergence-free approximation, which states that compressibility effects can be safely ignored. In microscale flows, the term $\rho_0 \langle \partial_t \boldsymbol{v}_0 \rangle$ in (B5*b*) can be neglected. Consequently, our governing equations reduce to

$$\boldsymbol{\nabla} \cdot \langle \boldsymbol{v}_0 \rangle = 0, \tag{B7a}$$

$$-\boldsymbol{\nabla} \langle p_0 \rangle + \eta \nabla^2 \langle \boldsymbol{v}_0 \rangle - \boldsymbol{\nabla} \cdot \langle \rho_0 \boldsymbol{v}_1 \boldsymbol{v}_1 \rangle + \langle \rho_0 \boldsymbol{g} \rangle = 0, \tag{B7b}$$

$$\langle \partial_t s_0 \rangle + \langle \boldsymbol{v}_0 \cdot \boldsymbol{\nabla} s_0 \rangle = D \nabla^2 \langle s_0 \rangle. \tag{B7c}$$

Hence, the body force due to acoustic fields is construed as

$$\boldsymbol{f}_{ac} = -\boldsymbol{\nabla} \cdot \langle \rho_0 \boldsymbol{v}_1 \boldsymbol{v}_1 \rangle. \tag{B8}$$

Appendix C. First-order equations in frequency domain

The first-order equations, which give rise to the first-order fields, ((2.3) in the main text) are specified to be solved in the frequency domain on the fast time scale. As we are solving the governing equations at a particular frequency for all acoustic phenomena, they can be rewritten as

$$-\mathrm{i}\omega\rho_1 = -\nabla\cdot(\rho_0\boldsymbol{v}_1), \tag{C1a}$$

$$-\mathrm{i}\omega\rho_0\boldsymbol{v}_1 = -\nabla p_1 + \eta\nabla^2\boldsymbol{v}_1 + \beta\eta\nabla(\nabla\cdot\boldsymbol{v}_1), \tag{C1b}$$

$$-\mathrm{i}\omega s_1 + \boldsymbol{v}_1\cdot\nabla s_0 = 0, \tag{C1c}$$

$$-\mathrm{i}\omega\rho_0\kappa_0 p_1 = -\mathrm{i}\omega\rho_1 + \boldsymbol{v}_1\cdot\nabla\rho_0. \tag{C1d}$$

Also, combining (C1*a*) and (C1*d*) we get

$$-\mathrm{i}\omega\kappa_0 p_1 = -\nabla\cdot\boldsymbol{v}_1, \tag{C1e}$$

where p_1 is the first-order pressure field, ρ_1 refers to the first-order density field, $\boldsymbol{v}_1$ is the first-order velocity field, ω is the angular frequency, η is the dynamic viscosity of the fluid, ξ is the volume fluid viscosity, $\beta = (\xi/\eta) + (1/3)$, s is the solute concentration and D is the diffusivity. In the time-dependent domain (C1*e*) can be written as $\kappa_0\partial_t p_1 = -\nabla\cdot\boldsymbol{v}_1$.

Appendix D. Variation of first-order and second-order fields for different configurations

In support of the analytical calculations and numerical simulations for the theory proposed, the profiles of the first-order velocity and pressure fields are shown below.

From figure 6 it is observed that the first-order fields ($\boldsymbol{v}_1$ and p_1) are highly configuration dependent, thus they change with respect to time, which supports the fact that the assumption of E_{ac} being constant is incorrect. In figure 7, it is seen that the magnitude of the second-order velocity $\langle\boldsymbol{v}_2\rangle$ is very high as the fluids evolve by an advection process to settle to a stable configuration. Also, it is noticed that the second-order pressure $\langle p_2\rangle$ is also significantly high. This is because of the large magnitude of p_1 at this instant that increases E_{ac} drastically, which in turn affects $\langle p_2\rangle$ and $\langle\boldsymbol{v}_2\rangle$. The second-order streaming velocity in this study refers to the time-averaged Eulerian streaming velocity. It can also be better represented by the Lagrangian streaming velocity. The Eulerian and Lagrangian velocities are related using Stokes drift (Hamilton, Ilinskii & Zabolotskaya 2003; Pavlic & Dual 2021).

From figure 8, it is evident that the first-order velocity has a large variation within the thin viscous boundary layer due to the no-slip condition whereas the first-order pressure remains the same inside and outside the boundary layer. Thus the acoustic standing wave relation $p_1 = p_a\sin(kx)$ and $\boldsymbol{v}_1 = (p_a/i\rho_0 c_0)\cos(kx)$ (where $k = 2\pi/\lambda$ is wavenumber and $\lambda \approx 2w$) holds good only outside the boundary layer.

Figure 9 shows the relocation of immiscible fluids under acoustic fields. Here also, the first-order fields ($\boldsymbol{v}_1$ and p_1) are highly configuration dependent. Due to the application of a two-dimensional standing wave, the pressure nodes are not formed at the centre of the channel as a vertical line (figure 9*c*) unlike for miscible fluids (figure 6*c*).

Appendix E. Fluid interface at the node for inhomogeneous fluids

In order to study the effect of the acoustic body force term alone, the influence of gravity has been excluded to avoid stratification. From figure 10, we see that acoustic relocation

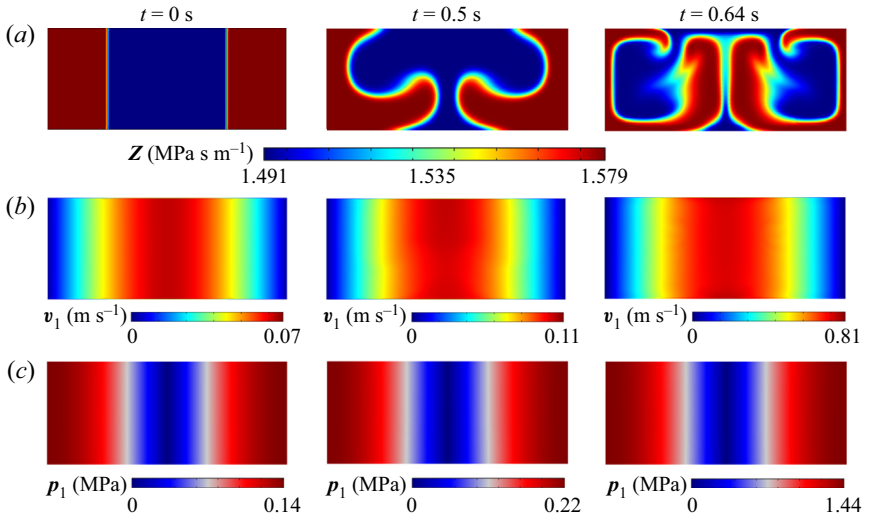

Figure 6. (*a*) Impedance profile for relocation of an unstable configuration to a stable configuration with $d = 0.261$ nm and $\nu = 1.96$ MHz. Initially (t=0s), there is low impedance DI water (blue) at the centre and high impedance 10 % Ficoll PM70 (red) at the sides. (*b*) Corresponding first-order velocity v_1. (*c*) Corresponding first-order pressure p_1. The microchannel width $w = 380$ µm and height $h = 160$ µm.

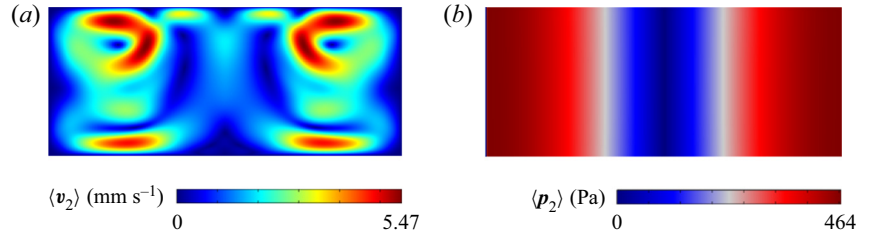

Figure 7. Corresponding (*a*) second-order velocity ($\langle \boldsymbol{v}_2 \rangle$) and (*b*) second-order pressure ($\langle p_2 \rangle$) profile at $t = 0.64$ s for the fluid configuration considered in figure (1).

does not occur in the case of inhomogeneous fluids when the fluid interface is at the node. Acoustic streaming can disturb the interface location, as shown at $t = 1.4$ s, after which the acoustic body force tries to stabilize the configuration.

Appendix F. Analysing the body force term f_{ac} in detail

The body force $\boldsymbol{f}_{ac} = -\boldsymbol{\nabla} \cdot \langle \rho_0 \boldsymbol{v}_1 \boldsymbol{v}_1 \rangle$ derived in the main text is analysed in detail by splitting it as

$$-\boldsymbol{\nabla} \cdot \langle \rho_0 \boldsymbol{v}_1 \boldsymbol{v}_1 \rangle = -\rho_0 \langle \boldsymbol{v}_1 \cdot \boldsymbol{\nabla} \boldsymbol{v}_1 \rangle - \langle \rho_1 \partial_t \boldsymbol{v}_1 \rangle. \tag{F1}$$

Consider the first term $-\rho_0 \langle \boldsymbol{v}_1 \cdot \boldsymbol{\nabla} \boldsymbol{v}_1 \rangle$. Using the identity $\boldsymbol{A}, \boldsymbol{A} \cdot \boldsymbol{\nabla} \boldsymbol{A} = \boldsymbol{\nabla}(\boldsymbol{A}^2/2) - \boldsymbol{A} \times (\boldsymbol{\nabla} \times \boldsymbol{A})$, it can be written as

$$-\rho_0 \langle \boldsymbol{v}_1 \cdot \boldsymbol{\nabla} \boldsymbol{v}_1 \rangle = -\frac{1}{2} \rho_0 \boldsymbol{\nabla} \langle |\boldsymbol{v}_1^2| \rangle + \rho_0 \langle \boldsymbol{v}_1 \times (\boldsymbol{\nabla} \times \boldsymbol{v}_1) \rangle, \tag{F2a}$$

$$-\rho_0 \langle \boldsymbol{v}_1 \cdot \boldsymbol{\nabla} \boldsymbol{v}_1 \rangle = \frac{-1}{2\rho_0} \boldsymbol{\nabla} \langle |\rho_0 \boldsymbol{v}_1|^2 \rangle + \langle |\boldsymbol{v}_1|^2 \rangle \boldsymbol{\nabla} \rho_0 + \rho_0 \langle \boldsymbol{v}_1 \times (\boldsymbol{\nabla} \times \boldsymbol{v}_1) \rangle. \tag{F2b}$$

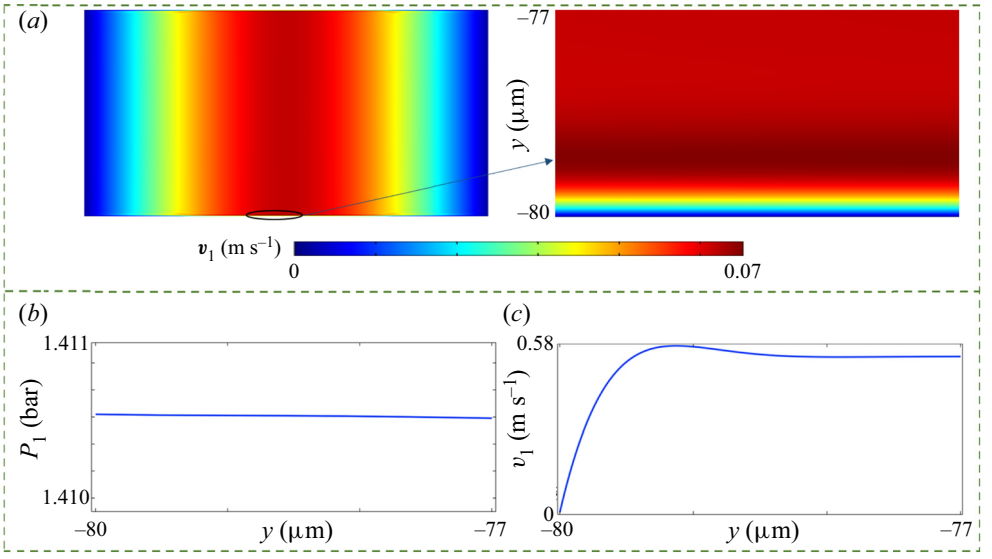

Figure 8. (*a*) Variation of first-order velocity at t=0 s near the boundary layer. Plots for variation of (*b*) first-order pressure p_1 and (*c*) first-order velocity v_1 in the direction of height.

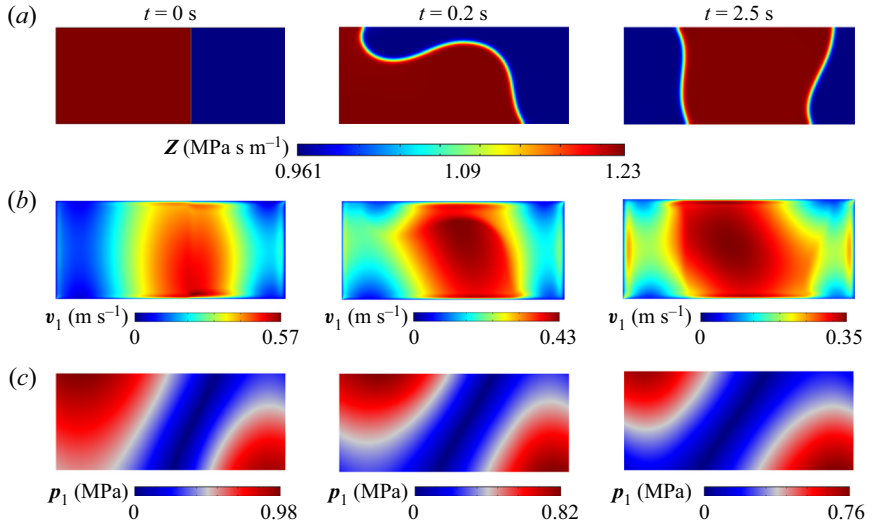

Figure 9. Results of relocation of immiscible fluids by actuating all walls of a microchannel (two-dimensional), consisting of high impedance mineral oil (red) and low impedance silicone oil (blue) with a surface tension of 1 mN m^{-1}. The wall is actuated with a displacement $d = 15$ nm at a frequency of 2.1 MHz. (*a*) Impedance profile. (*b*) First-order velocity profile $\boldsymbol{v}_1$. (*c*) First-order pressure profile p_1. The microchannel is of width $w = 360$ μm and height $h = 160$ μm.

Now consider the second term on the right-hand side of (F1), $-\langle \rho_1 \partial_t \boldsymbol{v}_1 \rangle$. Using $\partial_t(\rho_1 \boldsymbol{v}_1) = 0$, we have $-\langle \rho_1 \partial_t \boldsymbol{v}_1 \rangle = \langle \boldsymbol{v}_1 \partial_t \rho_1 \rangle$ and from the first-order continuity equation, we have $\partial_t \rho_1 = -\boldsymbol{\nabla} \cdot (\rho_0 \boldsymbol{v}_1)$. Substituting these and using the identity $\boldsymbol{\nabla} \cdot (AB) = B \cdot \boldsymbol{\nabla}(A) + A\boldsymbol{\nabla} \cdot (B)$, (where A and B are two vectors), we get

$$-\langle \boldsymbol{v}_1 \boldsymbol{\nabla} \cdot (\rho_0 \boldsymbol{v}_1) \rangle = -\langle \boldsymbol{v}_1 (\boldsymbol{v}_1 \cdot \boldsymbol{\nabla} \rho_0) \rangle - \langle \rho_0 \boldsymbol{v}_1 \boldsymbol{\nabla} \cdot \boldsymbol{v}_1 \rangle. \tag{F3}$$

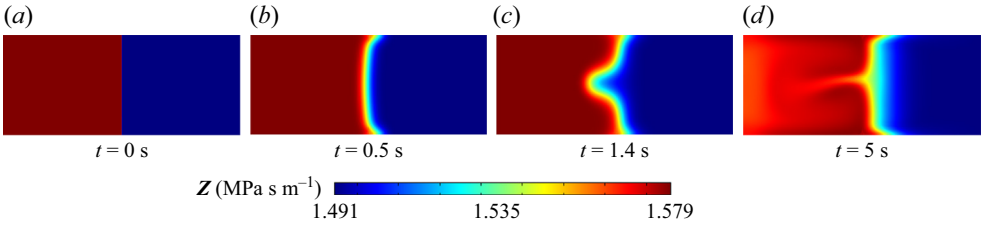

Figure 10. No relocation of inhomogeneous fluid when the interface is at node.

From $\kappa_0\partial_t p_1 = -\nabla\cdot\boldsymbol{v}_1$, the second term on the right-hand side of (F3) can be simplified as $-\langle\rho_0\boldsymbol{v}_1\nabla\cdot\boldsymbol{v}_1\rangle = \langle\rho_0\boldsymbol{v}_1(\kappa_0\partial_t p_1)\rangle = -\langle\kappa_0 p_1(\rho_0\partial_t\boldsymbol{v}_1)\rangle$ (since $\langle f_1(\partial_t g_1)\rangle = -\langle g_1(\partial_t f_1)\rangle$ is valid for time-harmonic fields f_1 and g_1). Now, using the first-order momentum equation ($\rho_0\partial_t\boldsymbol{v}_1 = -\nabla p_1 + \eta\nabla^2\boldsymbol{v}_1 + \beta\eta\nabla(\nabla\cdot\boldsymbol{v}_1)$), (F3) reduces to

$$-\langle\boldsymbol{v}_1\nabla\cdot(\rho_0\boldsymbol{v}_1)\rangle = \langle-\boldsymbol{v}_1(\boldsymbol{v}_1\cdot\nabla\rho_0)\rangle - \langle\kappa_0 p_1(-\nabla p_1 + \eta\nabla^2\boldsymbol{v}_1 + \beta\eta\nabla(\nabla\cdot\boldsymbol{v}_1))\rangle, \tag{F4a}$$

$$-\langle\boldsymbol{v}_1\nabla\cdot(\rho_0\boldsymbol{v}_1)\rangle = \tfrac{1}{2}\kappa_0\nabla\langle|p_1^2|\rangle - \langle\boldsymbol{v}_1(\boldsymbol{v}_1\cdot\nabla\rho_0)\rangle - \langle\kappa_0 p_1(\eta\nabla^2\boldsymbol{v}_1 + \beta\eta\nabla(\nabla\cdot\boldsymbol{v}_1))\rangle. \tag{F4b}$$

Adding (F2*b*) and (F4*b*)

$$\boldsymbol{f}_{ac} = \frac{1}{2}\kappa_0\nabla\langle|p_1^2|\rangle - \frac{1}{2\rho_0}\nabla\langle|\rho_0\boldsymbol{v}_1|^2\rangle + \langle|\boldsymbol{v}_1|^2\rangle\nabla\rho_0 + \langle\boldsymbol{v}_1\times\nabla\times(\rho_0\boldsymbol{v}_1)\rangle$$
$$-\langle\boldsymbol{v}_1(\boldsymbol{v}_1\cdot\nabla\rho_0)\rangle - \langle\kappa_0 p_1(\eta\nabla^2\boldsymbol{v}_1 + \beta\eta\nabla(\nabla\cdot\boldsymbol{v}_1))\rangle, \tag{F5a}$$

$$= \frac{1}{2}\kappa_0\nabla\langle|p_1^2|\rangle - \frac{1}{2\rho_0}\nabla\langle|\rho_0\boldsymbol{v}_1|^2\rangle + \langle\boldsymbol{v}_1\times\nabla\times(\rho_0\boldsymbol{v}_1)\rangle - \langle\kappa_0 p_1(\eta\nabla^2\boldsymbol{v}_1 + \beta\eta\nabla(\nabla\cdot\boldsymbol{v}_1))\rangle, \tag{F5b}$$

$$= \tfrac{1}{2}\nabla(\kappa_0\langle|p_1|^2\rangle - \rho_0\langle|\boldsymbol{v}_1|^2\rangle) + \{\langle\boldsymbol{v}_1\times\nabla\times(\rho_0\boldsymbol{v}_1)\rangle\}$$
$$-\tfrac{1}{2}[\langle|p_1|^2\rangle\nabla\kappa_0 + \langle|\boldsymbol{v}_1|^2\rangle\nabla\rho_0] - \langle(\kappa_0 p_1)(\eta\nabla^2\boldsymbol{v}_1 + \beta\eta\nabla(\nabla\cdot\boldsymbol{v}_1))\rangle. \tag{F5c}$$

For an acoustic wave propagating in the medium with frequency in the range of MHz, the orders of magnitude of individual parameters are wavenumber $k\sim O(10^4)$, $\rho_0\sim O(10^3)$, $\delta\sim O(10^{-6})$, $c_0\sim O(10^3)$, $\eta\sim O(10^{-3})$ and $p_1\sim\rho_0 c_0\boldsymbol{v}_1$ (where u_1 and v_1 denote x and y components of first-order velocity). The order of magnitude analysis results in, outside the boundary layer,

$$\frac{1}{2}\nabla(\kappa_0\langle|p_1|^2\rangle - \rho_0\langle|\boldsymbol{v}_1|^2\rangle \sim \frac{\rho_0 k u_1^2}{2} \sim O(10^6)(u_1^2), \tag{F6a}$$

$$-\langle(\kappa_0 p_1)(\eta\nabla^2\boldsymbol{v}_1 + \beta\eta\nabla(\nabla\cdot\boldsymbol{v}_1))\rangle \sim \frac{\eta k^2 u_1^2}{c_0} \sim O(10^2)(u_1^2). \tag{F6b}$$

Inside the boundary layer,

$$\{\langle\boldsymbol{v}_1\times\nabla\times(\rho_0\boldsymbol{v}_1)\rangle\} \sim \frac{\rho_0 u_1^2}{\delta} \sim O(10^9)(u_1^2), \tag{F6c}$$

$$-\langle(\kappa_0 p_1)(\eta\nabla^2\boldsymbol{v}_1 + \beta\eta\nabla(\nabla\cdot\boldsymbol{v}_1))\rangle \sim \frac{\eta u_1^2}{c_0\delta^2} \sim O(10^6)(u_1^2). \tag{F6d}$$

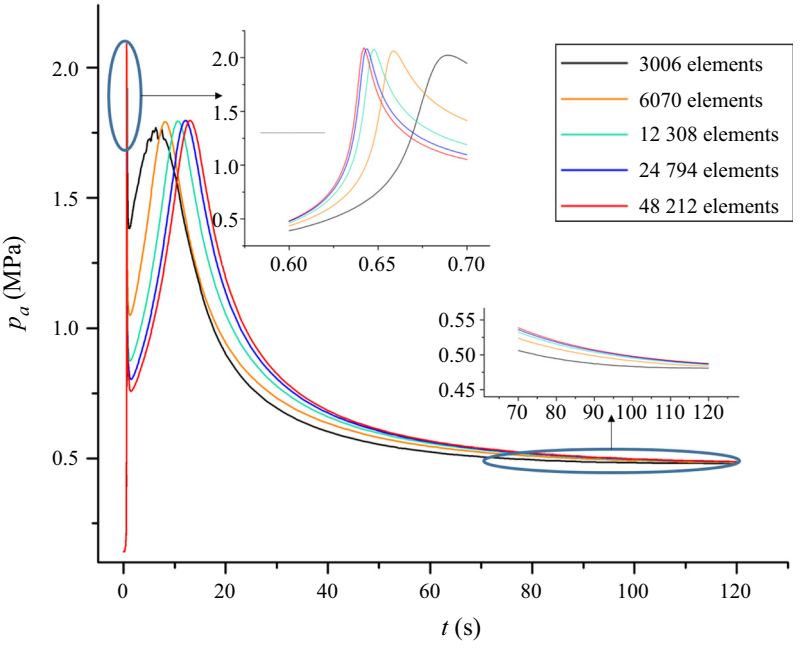

Figure 11. Mesh convergence analysis for first-order pressure amplitude p_a.

From the above arguments, we can conclude that the last term in (F5*c*) is insignificant inside as well as outside the boundary layer on comparing the magnitudes of acoustic parameters with those of other terms, thus we can certainly neglect this term to proceed further. Hence, the equation reduces to

$$\boldsymbol{f}_{ac} = -\boldsymbol{\nabla}\cdot\langle\rho_0\boldsymbol{v}_1\boldsymbol{v}_1\rangle = \tfrac{1}{2}\boldsymbol{\nabla}(\kappa_0\langle|p_1|^2\rangle - \rho_0\langle|\boldsymbol{v}_1|^2\rangle) + \{\langle\boldsymbol{v}_1\times\boldsymbol{\nabla}\times(\rho_0\boldsymbol{v}_1)\rangle\} - \tfrac{1}{2}[\langle|p_1|^2\rangle\boldsymbol{\nabla}\kappa_0 + \langle|\boldsymbol{v}_1|^2\rangle\boldsymbol{\nabla}\rho_0]. \tag{F7}$$

Appendix G. Mesh convergence and numerical uncertainty

The mesh convergence analysis is performed as shown in figures 11 and 12 to determine the number of grids large enough for all dependent variables to converge, ensuring a mesh-independent result. The dark blue line, which indicates a mesh constituting of 24 794 triangular grid elements (maximum element size of about 2.655 μm), is chosen as a trade-off between computational time and accuracy.

The discretization error and numerical uncertainty for this mesh is estimated using the Richardson extrapolation method. The discretization error is given as (Freitas 2002; Phillips & Roy 2014)

$$\varepsilon \approx [(f_f - f_c)/f_f]/[r^p - 1], \tag{G1}$$

where $p = \ln[(f_m - f_c)/(f_f - f_m)]/\ln[r]$ is the order of the convergence rate, subscript f refers to the fine grid solution (24 794 elements), c refers to the course grid solution (6070 elements), m refers to the medium grid solution (12 308 elements) and r is the ratio of grid spacings. For numerical solutions on the fine grid, grid convergence indices for the pressure amplitude and second-order velocity are calculated to be 1.028 % and 2.793 % respectively. Thus, the numerical uncertainty for pressure amplitude is $p_a \pm 0.01p_a$, and the second-order velocity is $\boldsymbol{v}_2 \pm 0.027\boldsymbol{v}_2$.

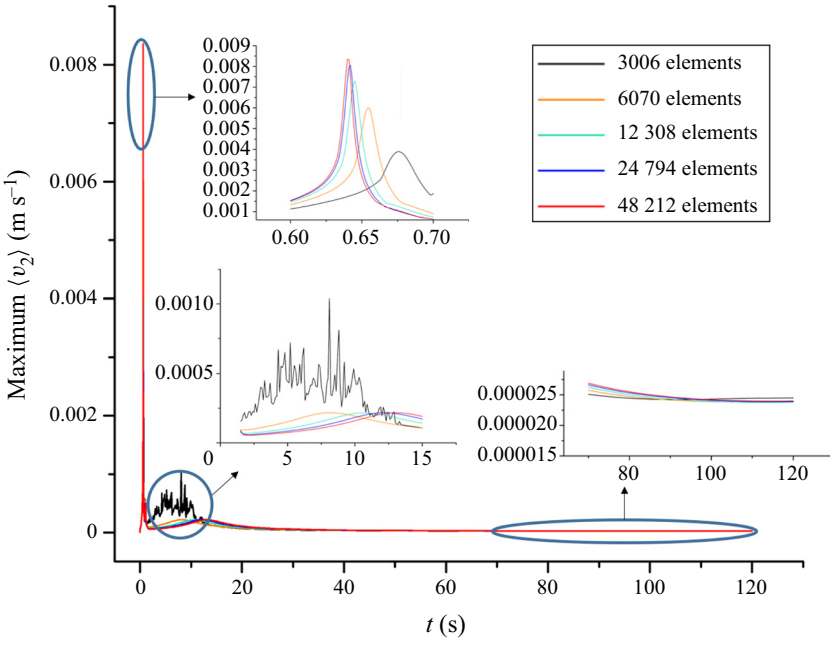

Figure 12. Mesh convergence analysis for maximum second-order velocity $\langle \boldsymbol{v}_2 \rangle$.

References

Ahmed, D., Ozcelik, A., Bojanala, N., Nama, N., Upadhyay, A., Chen, Y., Hanna-Rose, W. & Huang, T.J. 2016 Rotational manipulation of single cells and organisms using acoustic waves. *Nat. Commun.* **7**, 11085.

Augustsson, P., Karlsen, J.T., Su, H.-W., Bruus, H. & Voldman, J. 2016 Iso-acoustic focusing of cells for size-insensitive acousto-mechanical phenotyping. *Nat. Commun.* **7**, 11556.

Augustsson, P., Magnusson, C., Nordin, M., Lilja, H. & Laurell, T. 2012 Microfluidic, label-free enrichment of prostate cancer cells in blood based on acoustophoresis. *Anal. Chem.* **84** (18), 7954–7962.

Baasch, T., Doinikov, A.A. & Dual, Jürg 2020 Acoustic streaming outside and inside a fluid particle undergoing monopole and dipole oscillations. *Phys. Rev.* E **101** (1), 013108.

Baudoin, M. & Thomas, J.-L. 2020 Acoustic tweezers for particle and fluid micromanipulation. *Annu. Rev. Fluid Mech.* **52** (1), 205–234.

Bergmann, P.G. 2005 The wave equation in a medium with a variable index of refraction. *J. Acoust. Soc. Am.* **17** (4), 329–333.

Bradley, C.E. 1998 Acoustic streaming field structure: the influence of the radiator. *J. Acoust. Soc. Am.* **100** (3), 1399–1408.

Bruus, H. 2011 Acoustofluidics 2: perturbation theory and ultrasound resonance modes. *Lab on a Chip* **12** (1), 20–28.

Chen, Z., Pei, Z., Zhao, X., Zhang, J., Wei, J. & Hao, N. 2021 Acoustic microreactors for chemical engineering. *Chem. Engng J.* **433**, 133258.

Collins, D.J., Morahan, B., Garcia-Bustos, J., Doerig, C., Plebanski, M. & Neild, A. 2015 Two-dimensional single-cell patterning with one cell per well driven by surface acoustic waves. *Nat. Commun.* **6**, 8686.

Deshmukh, S., Brzozka, Z., Laurell, T. & Augustsson, P. 2014 Acoustic radiation forces at liquid interfaces impact the performance of acoustophoresis. *Lab on a Chip* **14** (17), 3394–3400.

Eckart, C. 1948 Vortices and streams caused by sound waves. *Phys. Rev.* **73** (1), 68–76.

Faraday, M. 1831 XVII. On a peculiar class of acoustical figures; and on certain forms assumed by groups of particles upon vibrating elastic surfaces. *Phil. Trans. R. Soc. Lond.* **121**, 299–340.

Freitas, C.J. 2002 The issue of numerical uncertainty. *Appl. Math. Model.* **26** (2), 237–248.

Friend, J. & Yeo, L.Y. 2011 Microscale acoustofluidics: microfluidics driven via acoustics and ultrasonics. *Rev. Mod. Phys.* **83** (2), 647–704.

GAUTAM, G.P., GURUNG, R., FENCL, F.A. & PIYASENA, M.E. 2018 Separation of sub-micron particles from micron particles using acoustic fluid relocation combined with acoustophoresis. *Anal. Bioanal. Chem.* **410** (25), 6561–6571.

HAMILTON, M.F., ILINSKII, Y.A. & ZABOLOTSKAYA, E.A. 2003 Acoustic streaming generated by standing waves in two-dimensional channels of arbitrary width. *J. Acoust. Soc. Am.* **113** (1), 153–160.

HEMACHANDRAN, E., HOQUE, S.Z., LAURELL, T. & SEN, A.K. 2021 Reversible stream drop transition in a microfluidic coflow system via on demand exposure to acoustic standing waves. *Phys. Rev. Lett.* **127** (13), 134501.

HEMACHANDRAN, E., KARTHICK, S., LAURELL, T. & SEN, A.K. 2019 Relocation of coflowing immiscible liquids under acoustic field in a microchannel. *Europhys. Lett.* **125** (5), 54002.

KARLSEN, J.T. 2018 Theory of nonlinear acoustic forces acting on fluids and particles in microsystems. In *DTU Research Database*. PhD Thesis, Technical University of Denmark.

KARLSEN, J.T., AUGUSTSSON, P. & BRUUS, H. 2016 Acoustic force density acting on inhomogeneous fluids in acoustic fields. *Phys. Rev. Lett.* **117** (11), 114504.

KARLSEN, J.T. & BRUUS, H. 2017 Acoustic tweezing and patterning of concentration fields in microfluidics. *Phys. Rev. Appl.* **7** (3), 034017.

KARLSEN, J.T., QIU, W., AUGUSTSSON, P. & BRUUS, H. 2018 Acoustic streaming and its suppression in inhomogeneous fluids. *Phys. Rev. Lett.* **120** (5), 054501.

KING, L.V. 1934 On the acoustic radiation pressure on spheres. *Proc. R. Soc. Lond.* A - *Math. Phys. Sci.* **147** (861), 212–240.

KUMAR, V., AZHARUDEEN, M., POTHURI, C. & SUBRAMANI, K. 2021 Heat transfer mechanism driven by acoustic body force under acoustic fields. *Phys. Rev. Fluids* **6** (7), 073501.

LANDAU, L.D. & LIFSHITZ, E.M. 1987 *Fluid Mechanics*. Pergamon.

LEE, K., SHAO, H., WEISSLEDER, R. & LEE, H. 2015 Acoustic purification of extracellular microvesicles. *ACS Nano* **9** (3), 2321–2327.

LI, P. & HUANG, T.J. 2019 Applications of acoustofluidics in bioanalytical chemistry. *Anal. Chem.* **91** (1), 757–767.

LI, P., *et al.* 2015 Acoustic separation of circulating tumor cells. *Proc. Natl Acad. Sci. USA* **112** (16), 4970–4975.

LIGHTHILL, S.J. 1978 Acoustic streaming. *J. Sound Vib.* **61** (3), 391–418.

MULLER, P.B. & BRUUS, H. 2014 Numerical study of thermoviscous effects in ultrasound-induced acoustic streaming in microchannels. *Phys. Rev.* E **90** (4), 043016.

NATH, A. & SEN, A.K. 2019 Acoustic behavior of a dense suspension in an inhomogeneous flow in a microchannel. *Phys. Rev. Appl.* **12** (5), 054009.

NYBORG, W.L. 2005 Acoustic streaming near a boundary. *J. Acoust. Soc. Am.* **30** (4), 329.

PAVLIC, A. & DUAL, JÜRG 2021 On the streaming in a microfluidic Kundt's tube. *J. Fluid Mech.* **911**, A28.

PETERSSON, F., ÅBERG, L., SWÄRD-NILSSON, A.-M. & LAURELL, T. 2007 Free flow acoustophoresis microfluidic-based mode of particle and cell separation. *Anal. Chem.* **79** (14), 5117–5123.

PHILLIPS, T.S. & ROY, C.J. 2014 Richardson extrapolation-based discretization uncertainty estimation for computational fluid dynamics. *Trans. ASME J. Fluids Engng* **136** (12), 121401.

POTHURI, C., AZHARUDEEN, M. & SUBRAMANI, K. 2019 Rapid mixing in microchannel using standing bulk acoustic waves. *Phys. Fluids* **31** (12), 122001.

QIU, W., KARLSEN, J.T., BRUUS, H. & AUGUSTSSON, P. 2019 Experimental characterization of acoustic streaming in gradients of density and compressibility. *Phys. Rev. Appl.* **11** (2), 024018.

RAYLEIGH, LORD 1884 On the circulation of air observed in Kundt's tubes, and on some allied acoustical problems. *Phil. Trans. R. Soc. Lond.* **175**, 1–21.

SUSLICK, K.S., DIDENKO, Y., FANG, M.M., HYEON, T., KOLBECK, K.J., WILLIAM B. MCNAMARA, I., MDLELENI, M.M. & WONG, M. 1999 Acoustic cavitation and its chemical consequences. *Phil. Trans. R. Soc. Lond.* A **357** (1751), 335–353.

VAN ASSCHE, D., REITHUBER, E., QIU, W., LAURELL, T., HENRIQUES-NORMARK, B., MELLROTH, P., OHLSSON, P. & AUGUSTSSON, P. 2020 Gradient acoustic focusing of sub-micron particles for separation of bacteria from blood lysate. *Sci. Rep.* **10**, 3670.

WIKLUND, M. 2012 Acoustofluidics 12: biocompatibility and cell viability in microfluidic acoustic resonators. *Lab on a Chip* **12** (11), 2018–2028.